Clinical Cancer Research

Subjugation of TGFβ Signaling by Human Papilloma Virus in Head and Neck Squamous Cell Carcinoma Shifts DNA Repair from Homologous Recombination to Alternative End Joining

Qi Liu[1], Lin Ma[1], Trevor Jones[1], Luis Palomero[2], Miquel Angel Pujana[2], Haydeliz Martinez-Ruiz[3], Patrick K. Ha[1], John Murnane[1], Isabel Cuartas[4], Joan Seoane[4], Michael Baumann[5,6], Annett Linge[5], and Mary Helen Barcellos-Hoff[1]

Abstract

Purpose: Following cytotoxic therapy, 70% of patients with human papillomavirus (HPV)-positive oropharyngeal head and neck squamous cell carcinoma (HNSCC) are alive at 5 years compared with 30% of those with similar HPV-negative cancer. Loss of TGFβ signaling is a poorly studied consequence of HPV that could contribute to patient outcome by compromising DNA repair.

Experimental Design: Human HNSCC cell lines ($n = 9$), patient-derived xenografts ($n = 9$), tissue microarray ($n = 194$), TCGA expression data ($n = 279$), and primary tumor specimens ($n = 10$) were used to define the relationship between TGFβ competency, response to DNA damage, and type of DNA repair.

Results: Analysis of HNSCC specimens *in situ* and *in vitro* showed that HPV associated with loss of TGFβ signaling that increased response to radiation or cisplatin. TGFβ suppressed miR-182, which inhibited both BRCA1, necessary for homologous recombination repair (HRR), and FOXO3, required for ATM kinase activity. TGFβ signaling blockade by either HPV or inhibitors released miR182 control, compromised HRR and increased response to PARP inhibition. Antagonizing miR-182 rescued the HRR deficit in HPV-positive cells. Loss of TGFβ signaling unexpectedly increased repair by error prone, alternative end-joining (alt-EJ).

Conclusions: HPV-positive HNSCC cells are unresponsive to TGFβ. Abrogated TGFβ signaling compromises repair by HRR and increases reliance on alt-EJ, which provides a mechanistic basis for sensitivity to PARP inhibitors. The effect of HPV in HNSCC provides critical validation of TGFβ's role in DNA repair proficiency and further raises the translational potential of TGFβ inhibitors in cancer therapy. *Clin Cancer Res; 24(23); 6001–14. ©2018 AACR.*

Introduction

The prognosis for patients with head and neck squamous cell carcinomas (HNSCCs) is associated with anatomical location, tumor characteristics, and patient history (1). Patients with oropharyngeal squamous cell carcinoma whose cancer is positive for human papillomavirus (HPV positive) have a markedly better prognosis compared with those patients whose tumors are HPV-negative (2). Recognition of this differential survival as a function of HPV in HNSCC has motivated dual goals to identify the mechanism by which HPV alters the DNA damage response (DDR) and to search for a means to achieve similar outcomes in HPV-negative HNSCC. HPV-positive cell lines are more sensitive to cytotoxic agents (3, 4) and exhibit decreased DNA repair capacity that may explain increased response to ionizing radiation (IR) and cisplatin, which are standard-of-care in HNSCC (5, 6). A specific DDR deficiency represents a vulnerability that could be exploited by cytotoxic therapy (7).

The cell-cycle machinery of proliferating cells is necessary for HPV replication. TGFβ profoundly suppresses epithelial cell proliferation. Studies in cervical cancer show that HPV encoded E5, E6, and E7 proteins bind to TGFβ receptors and signal transducers, resulting in their degradation, thereby releasing infected cells to proliferate (8). Although TGFβ is considered a canonical tumor suppressor, most cancers produce both abundant TGFβ and maintain competent TGFβ signaling (9). TGFβ binds a ubiquitous heteromeric complex of type I (TβRI) and type II receptors whose serine/threonine kinase activity initiate canonical signaling cascade via phosphorylation of SMAD (signaling mother against decapentaplegic peptide)

[1]Department of Radiation Oncology and Helen Diller Family Comprehensive Cancer Center, University of California, San Francisco, San Francisco, California. [2]ProCURE, Catalan Institute of Oncology, Bellvitge Institute for Biomedical Research (IDIBELL), L'Hospitalet del Llobregat, Barcelona, Spain. [3]Department of Cell Biology, New York University School of Medicine, New York, New York. [4]Vall d Hebron Institute of Oncology (VHIO), Institució Catalana de Recerca i Estudis Avançats (ICREA), Universitat Autònoma de Barcelona, CIBERONC, Barcelona, Spain. [5]German Cancer Research Center (DKFZ), Heidelberg, Germany. [6]German Cancer Consortium (DKTK), Partner Site Dresden, Germany; and Department of Radiotherapy and Radiation Oncology, University Hospital Carl Gustav Carus, Technische Universität Dresden, Germany.

Note: Supplementary data for this article are available at Clinical Cancer Research Online (http://clincancerres.aacrjournals.org/).

Corresponding Author: Mary Helen Barcellos-Hoff, University of California, San Francisco, 2340 Sutter Street, San Francisco, CA 94143. Phone: 415-476-8091; E-mail: MaryHelen.Barcellos-Hoff@ucsf.edu

doi: 10.1158/1078-0432.CCR-18-1346

Translational Relevance

The prognosis for patients with oropharyngeal HNSCC suggests that human papilloma virus (HPV) confers vulnerability to standard-of-care radiation and chemotherapy. Although HPV impairs p53 and retinoblastoma proteins, it can also compromise TGFβ signaling. We show that loss of TGFβ signaling leads to homologous recombination deficiency that increases sensitivity to radiation and chemotherapy, but the penultimate basis for poor DNA damage repair is the shift to error prone, alternative end-joining repair (alt-EJ) that requires both PARP1 and POLQ. The loss of TGFβ signaling in HPV-positive HNSCC is an experiment of nature that underscores a novel route by which TGFβ inhibitors can be exploited clinically in poor prognosis HPV-negative HNSCC.

2 and 3. SMAD 2/3 phosphorylation enables the formation of SMAD4 heteromeric complexes that bind SMAD-binding gene elements to control transcription. Notably, SMAD4 is frequently mutated or deleted in HPV-negative HNSCC (10), but whether HPV affects TGFβ signaling in HNSCC has not been examined.

Of its myriad roles, TGFβ's multiple inputs that maintain genomic stability is among the most poorly appreciated. Yuspa and colleagues first reported in 1996 that *Tgfb1* null keratinocytes exhibit profound genomic instability (11). Genetic deletion of *Tgfb1* or inhibiting TGFβ activity or signaling compromises DNA damage recognition and execution of canonical cell fate decisions, that is, repair, cycle arrest, and cell kill *in vivo* and *in vitro* (12). This is partly because TGFβ signaling is necessary for ataxia telangiectasia mutated (ATM) kinase activity (13) and ligase IV expression (14); both are important components of classical nonhomologous end joining (NHEJ) repair of DNA damage. TGFβ also regulates breast cancer early onset 1 (BRCA1; refs. 10, 15), which is a major component of homologous recombination repair (HRR). Together, the multiple mechanisms by which TGFβ controls DNA damage components raise the potential translational utility of pharmaceutical blockade of TGFβ signaling during cancer therapy (16, 17). Consistent with this, TGFβ inhibition promotes response to radiotherapy and/or chemotherapy in preclinical models of breast (18), brain (19–21), and lung cancer (22).

Here, we investigated whether HPV affects TGFβ signaling in HNSCC and if so, whether loss of TGFβ signaling underlies the responsiveness of HPV-positive HNSCC to cytotoxic therapy.

Materials and Methods

Cell lines

HNSCC cell lines were cultured in DMEM, supplemented with 10% FBS (HyClone), GlutaMax (Thermo Fisher Scientific), HEPES and 100 IU/mL streptomycin–penicillin (all Sigma-Aldrich unless otherwise indicated). Detroit562, SCC090, SCC154, and FADU were purchased from the ATCC. SCC47 and SCC104 were purchased from Millipore Sigma. HPV status of these cell lines was validated by PCR (23). All cells were maintained in a humidified incubator at 37°C and 5% CO_2. All cell lines were tested and deemed *Mycoplasma* free and their DNA identities validated by microsatellite markers for authentication (IDEXX). Cells were used within 10 passages and culture time restricted to a maximum of 6 weeks for all experiments after defrosting. Cells were maintained in exponential growth phase before sample preparation for each experiment.

Xenografts

Balb/c nude mice were purchased from Jackson Laboratory. All mouse experiments were approved by and performed according to the guidelines of the Institutional Animal Care Committee of the Vall d'Hebron Research Institute (Barcelona, Spain) in agreement with the European Union and national directives. Subcutaneous inoculation of 1×10^6 cells SAS in the flank was performed in 7-week-old mice with eight mice per group for treatments. Treatments began at day 10 postinoculation after randomization of tumor sizes. LY2157299 (15 mg/kg) was given by oral gavage twice a day, and olaparib (5 mg/kg) was given by oral gavage once a day. Tumor volume was measured daily using caliper method and weight monitored every day.

Treatments

TGFβ1 (500 pg/mL; R&D Systems, Inc.) was given in serum-free medium. Small-molecule inhibitors of the TβRI kinase, LY364947 (Calbiochem), and LY2157299 (Galunisertib; SelleckChem) were used at 2 μmol/L; a pan-isoform TGFβ neutralizing human mAb, GC-1008 (Fresolimumab), was used at 10 μg/mL. All TGFβ inhibitors were given for 24 to 48 hours prior to other treatments. PARP1/2 inhibitor olaparib (LC Laboratories) and PARP1 inhibitor AG14361 (SelleckChem) were used at 10 μmol/L and 1 μmol/L, respectively. ATM inhibitor KU55933, ATR inhibitor AZD6738, and DNA-PK inhibitor KU57788 (all SelleckChem) were used at 5 μmol/L, 0.5 μmol/L, and 1 μmol/L, respectively. Inhibitors against PARP, ATM, ATR, and DNA-PK were given 1 hour prior to irradiation. All the above compounds were dissolved in dimethyl sulfoxide (Sigma-Aldrich) and stored at −20°C for up to 6 months with protection from light. They were aliquoted for maximum 3× use to avoid thaw-freeze cycles. Cisplatin (Santa Cruz) was dissolved in 0.9% sodium chloride in water to achieve 4 mmol/L stock solution, stored at 4°C for up to 1 month with protection from light. Cells were irradiated to the indicated doses using 250 kV X-ray.

Cell survival and proliferation assays

Clonogenic survival assays were performed as described previously (18, 20, 22). Briefly, cells were trypsinized 3 hours after irradiation and diluted into the appropriate densities with single cell suspensions. Colonies were allowed to grow for a cell line–dependent time (10–20 days) followed by fixing with acetic acid/ methanol solution (volume ratio, 1:3) and staining with 0.5% crystal violet. Colonies containing at least 50 cells were scored under a bright field microscope. Plating efficiencies were calculated as colonies per number of cells plated, and surviving fractions as ratios of plating efficiencies for irradiated and unirradiated cells. Linear-quadratic formula (LQ): $\ln(SF) = -(\alpha D + \beta D^2)$, was used to fit survival curves and calculate dose enhancement ratio at 10% surviving fraction (DER).

Previously published cell proliferation assays were used (24). Relative response was calculated as number of treated cells divided by untreated control 5 to 7 days (consistent times were used for repeated experiments in each assay) after treatments measured by SYTO60 assay, a fluorescent nucleic acid stain, an ATP-based luminescence assay CellTiter-Glo (Promega) following the

manufacturer's protocol, or cell number counting with automated counter (Countess, Thermo Fisher Scientific). Short-term radiosensitizing factor at 2 Gy (SRF_{2Gy}) was calculated as the ratio of the cell fraction for IR alone and the cell fraction for combined drug/IR effect, corrected for the cell fraction for drug alone (24).

Flow cytometry assays

Cell-cycle distributions were investigated by flow cytometry analyses of DNA staining with propidium iodide (PI; Sigma-Aldrich) according to standard protocol. Cells were collected and washed twice with PBS, and then fixed in 80% cold ethanol. After washing twice in PBS, cells were incubated with 1 mg/mL ribonuclease (RNase) and 500 μg/mL PI, and then analyzed by flow cytometer (Calibur, BD Biosciences). Apoptotic cells were determined by annexin V flow as described previously (24). Cells were harvested 2 days after treatment and stained with annexin V with Alexa Fluor 488 conjugate and PI according to the manufacturer's protocol (Thermo Fisher Scientific). Data were analyzed by FlowJo.

Tissue microarray

The tissue microarray was generated within a retrospective study of the German Cancer Consortium Radiation Oncology Group (DKTK-ROG) and consists of up to three tissue cores of the untreated tumor and one or two cores of the adjacent tissue from 221 patients who were diagnosed with locally advanced HNSCC. All patients received postoperative, state-of-the-art cisplatin-based radiochemotherapy, and their inclusion criteria have been described previously (2). For this study, tissues of 194 patients were evaluable. HPV DNA analyses of the tumors were part of a previous publication, methods were described previously (2).

Explant specimens

Explants of HNSCC patient-derived xenografts (PDXs) were collected from mice in which tumors were grown. Primary patient tumor tissues were collected during surgery. All specimens were kept in DMEM and transported on ice with HPV status blinded to experimenters. Explants were established within 5 hours on floating rafts as described previously (25). On day 1, explants were dissected and distributed for treatments with or without TβRI inhibitor for 24 hours prior to irradiation with the indicated dose. At selected time points, samples were embedded in optimum cutting temperature compound (Sigma Aldrich) and frozen on dry ice. Specimens and slides of cryosections were kept at −80°C.

Immunofluorescence and microscopy

Staining and visualization of DDR foci was performed as described previously (22). Cells were plated on chamber slides. For HNSCC PDX and primary patient tumor explant analyses, slides were defrosted at room temperature before immunostaining. Samples were fixed with 4% paraformaldehyde for 15 minutes, permeabilized with 0.5% TritonX-100, and blocked with 0.5% casein in PBS. Samples were then incubated with γH2AX mouse mAb (EMD Millipore) at 1:500 dilution, and primary rabbit polyclonal antibodies against RAD51 (Santa Cruz) at 1:200, 53BP1 (Bethyl) at 1:200, Geminin (Abcam) at 1:200, or phospho-SMAD2 on serine 465/467 at 1:200 (Cell Signaling) at room temperature for 2 hours or 4°C overnight. After 3× washes with PBS, secondary antibody including donkey anti-rabbit IgG (Alexa Fluor 488/555, Invitrogen) and donkey anti-mouse IgG (Alexa Fluor 488/555, Invitrogen) was incubated for 1 hour. Cell nuclei were counterstained with 4′,6-diamidino-2-phenylindole, dihydrochloride (DAPI). Slides were mounted in Vectashield (Sigma). A 40× objective with 0.95 numerical aperture was used on a Zeiss Axiovert equipped with epifluorescence. In-home developed macros or Findfoci plugins (26) in the open source platform Fiji-ImageJ (NIH, Bethesda, MA) were used for image analyses of 8-bit images for each channel of fluorescence.

For the patient tissue array (27), intensity of p-SMAD2 was scored by three observers blinded to tissue identity according to the following criteria: level 1, no p-SMAD2 signal (negative, −); level 2, a little p-SMAD2 signal (positive, +); level 3, a medium p-SMAD2 signal (positive, ++); and level 4, a strong p-SMAD2 signal (positive, +++). The independent scores were averaged.

Western blotting

Proteins from exponentially growing cells were extracted on ice by RIPA containing protease and phosphatase inhibitor cocktails (Sigma Aldrich), quantified with bicinchoninic acid protein assay (Thermo Fisher Scientific). Forty to 100 μg was electrophoresed on 4% to 15% gradient gels from BioRad and transblotted on fluorescence-optimized PVDF membrane (Merck Millipore). Primary antibodies to BRCA1 N-terminus (a gift from Dr. Chodosh) or C-terminus (Santa Cruz), FOXO3 (Cell Signaling), ATM (GeneTex), p-ATM (Ser-1981, Abcam), or β-actin (Abcam) were incubated with the membrane followed by incubation with secondary antibodies (Odyssey) and scanned on the Odyssey LICOR system.

Immunoprecipitation

Cell lysates were prepared using specialized lysis buffer (Thermo Fisher Scientific), and protein G Sepharose beads were used for immunoprecipitation following the manufacturer's instructions (GE Healthcare) using rabbit mAb to FOXO3 (Cell Signaling) or ATM (GeneTex). The presence of ATM and p-ATM, or FOXO3 was probed by immunoblotting.

qRT-PCR

Total RNA was extracted from samples using the TRizol reagent (Invitrogen) and miRNA Easy Mini Kit (Qiagen) according to the manufacturer's instructions. cDNA was synthesized from 1 μg of RNA using the SuperScript III First-Strand Synthesis System (Invitrogen). qRT-PCR was performed using SYBR Green Mix (Applied Biosystems), according to the manufacturer's instructions. Primers with published sequences (15) were purchased from Sigma-Aldrich. Expression of genes of interest was normalized against expression of *GAPDH*. qRT-PCR analyses of miR-182 were performed using miRNA-specific TaqMan MicroRNA Assay Kit; 12.5 ng of total RNA was reverse transcribed using the corresponding RT Primer and the TaqMan MicroRNA Reverse Transcription Kit (Applied Biosystems). TaqMan PCR primers and the TaqMan Universal PCR Master Mix were added to reverse transcribed products for PCR analyses (Applied Biosystems). RNU44 was used for normalization of input RNA/cDNA levels. Data were analyzed using the comparative C_t method for quantification of transcripts.

Transfections

miR-182 mimic (50 nmol/L) or antagomir (200 nmol/L; i.e., anti-miR) was transfected into cells overnight in parallel

with non-targeting miRNA control (mirVana, Thermo Fisher Scientific). Published *FOXO3*-expressing plasmid with pCMV5 vector (Addgene) was transfected overnight into SAS cell line (28). Validated shRNA lentiviral transduction particles with pLKO.1 vector (Sigma Aldrich) were used to knock-down SMAD4 or POLQ in SAS cell line, with control cells prepared in parallel using vector control lentiviral particles. Cells were infected with 8 μg/mL polybrene overnight and grown in 2 μg/mL puromycin for selection. Lipofectamine 3000 Transfection Kit (Invitrogen) was used according to the manufacturer's instructions. Western blotting to determine protein levels of targeted genes and subsequent experiments were carried out 48 hours after transfection.

DSB repair reporter assay

DNA repair reporters of HRR (pDRGFP) or alt-EJ (EJ2GFP-puro) were stably integrated into clones of the SAS cell line using the published plasmid constructs (29, 30). To establish reporter cell clones, plasmids linearized with appropriate restriction enzyme were transfected into exponentially growing SAS cells using Lipofectamine 3000 in Opti-MEM. Cells were then selected in 2 μg/mL puromycin containing medium. Single cell clones were established in 96-well plates with one cell per well. pQCXIH-I-SceI was packaged into retroviral vectors for infection as described previously (31). Infected cells were selected in culture medium with 400 μg/mL hygromycin for 10 days. For analyses, the treated cells were trypsinized and maintained on ice before flow cytometry used to determine the fraction of GFP-positive cells. Propidium iodide staining was used to exclude dead cells from analyses.

Comet assay

Comet assay was performed according to the manufacturer's protocol (Trivigen). Tumor explants after treatment were chopped into small pieces for enzymatic disaggregation including 1.5 mg/mL collagenase and 0.25% trypsin at 37°C for 1 hour (Thermo Fisher Scientific). A cell strainer with 40-μm pores was used to obtain single-cell suspension for comet assay. Single-cell gel electrophoresis was performed at 19 V for 40 minutes. SYBR Gold–stained DNA comets were imaged with a Zeiss fluorescence microscope. Images were analyzed using Fiji-ImageJ with OpenComet (32). The Olive tail moments of at least 100 cells were determined in each sample by OpenComet.

TCGA and gene expression analyses

Clinical and gene expression data of HNSCC were obtained from cBioPortal for Cancer Genomics (http://www.cbioportal.org/public-portal/) and from the corresponding TCGA publication (33). A chronic TGFβ signature was defined using a nonmalignant epithelial cell line, MCF10A, that were exposed to TGFβ or LY364957 for 7 days and analyzed using Affymetrix gene expression microarray to identify genes with more than twofold change that were reciprocally regulated following chronic TGFβ treatment versus signaling inhibition. The RNA-seq TCGA data were used for correlation (based on Pearson correlation coefficient), hierarchical clustering (based on Euclidean distance), and survival analyses. The association with survival was computed in R software (*survfit* package) using multivariate Cox regression analyses adjusted by age, gender, tumor stage, and smoking status. The single-sample gene set enrichment analysis (ssGSEA) scores were computed using the GSVA package in Bioconductor (34).

Statistical analyses

The data were analyzed by GraphPad Prism 6. Bars or data points represent means based on at least three independent experiments with error bars indicating standard error or medians with 95% confidence intervals as indicated in figure legends. Two-tailed Student t test or Mann–Whitney U test was used for statistical comparisons and considered significantly different at $P < 0.05$. F-test was used to test the clonogenic survival effect after treatments by assessing coefficients α and β in derived formula by LQ fitting. P values are indicated in the figures as follows: ***, $P < 0.005$; **, $P < 0.01$; *, $P < 0.05$.

Study approval

Patient specimens were obtained with written consent from each patient in accordance with the ethics guidelines for research in the United States (protocols # 14-15342, approved by the IRB committee of UCSF) and in Germany (protocol# EK299092012, approved by the IRB committee of the DKTK partner site and subsequently by the IRB committees of all other DKTK partner sites).

Results

TGFβ signaling is decreased in HPV-positive HNSCC

We first sought to determine using data from HNSCC TCGA, of which 13% ($n = 36$) are HPV-positive (33), whether TGFβ signaling is associated with HPV status. We derived a chronic TGFβ expression signature in nonmalignant MCF10A epithelial cells treated for 7 days with either TGFβ or a small molecule inhibitor of TβRI kinase, LY364947 (Supplementary Fig. S1A). Thirty genes that were induced by at least twofold by TGFβ and blocked by LY364957 were expressed in HNSCC and used for supervised clustering. Almost all HPV-positive cancers were clustered in the clade with low expression of TGFβ-induced genes (Fig. 1A). The negative correlation suggests that TGFβ signaling is decreased in HPV-positive HNSCC.

Next, we sought to validate the association between HPV status and TGFβ signaling in a panel of HNSCC cell lines (Supplementary Fig. S1B). TβRI-mediated phosphorylation of SMAD 2 and 3 initiates TGFβ signal transduction. Protein levels of SMAD 2 and 3 and TGFβ type I and II receptors were similar among three HPV-negative and two HPV-positive cell lines (Supplementary Fig. S1C), however none of the cell lines were growth inhibited by TGFβ treatment. We assessed canonical signaling by localizing nuclear phosphorylated SMAD2 (p-SMAD2) in cells treated briefly with exogenous TGFβ. The increased p-SMAD2 was blocked by treating cells with TβRI kinase inhibitor LY364957 in an HPV-negative cell line, as expected. In contrast, TGFβ treatment did not increase in p-SMAD2 in an HPV-positive cell line (Fig. 1B). As a group, HPV-positive cell lines showed minimal response to TGFβ compared with HPV-negative cell lines (Fig. 1C and D).

We then tested p-SMAD2 response following acute TGFβ treatment of explants of HNSCC PDX (Supplementary Fig. S1D). As found in the cell lines, TGFβ elicited more robust nuclear p-SMAD2 in HPV-negative PDX compared with HPV-positive PDX (Fig. 1E). Overall, the levels of p-SMAD2 of HPV-positive PDX ($n = 5$) were significantly less than that of HPV-negative PDX ($n = 4$). Finally, we performed semi quantitative evaluation

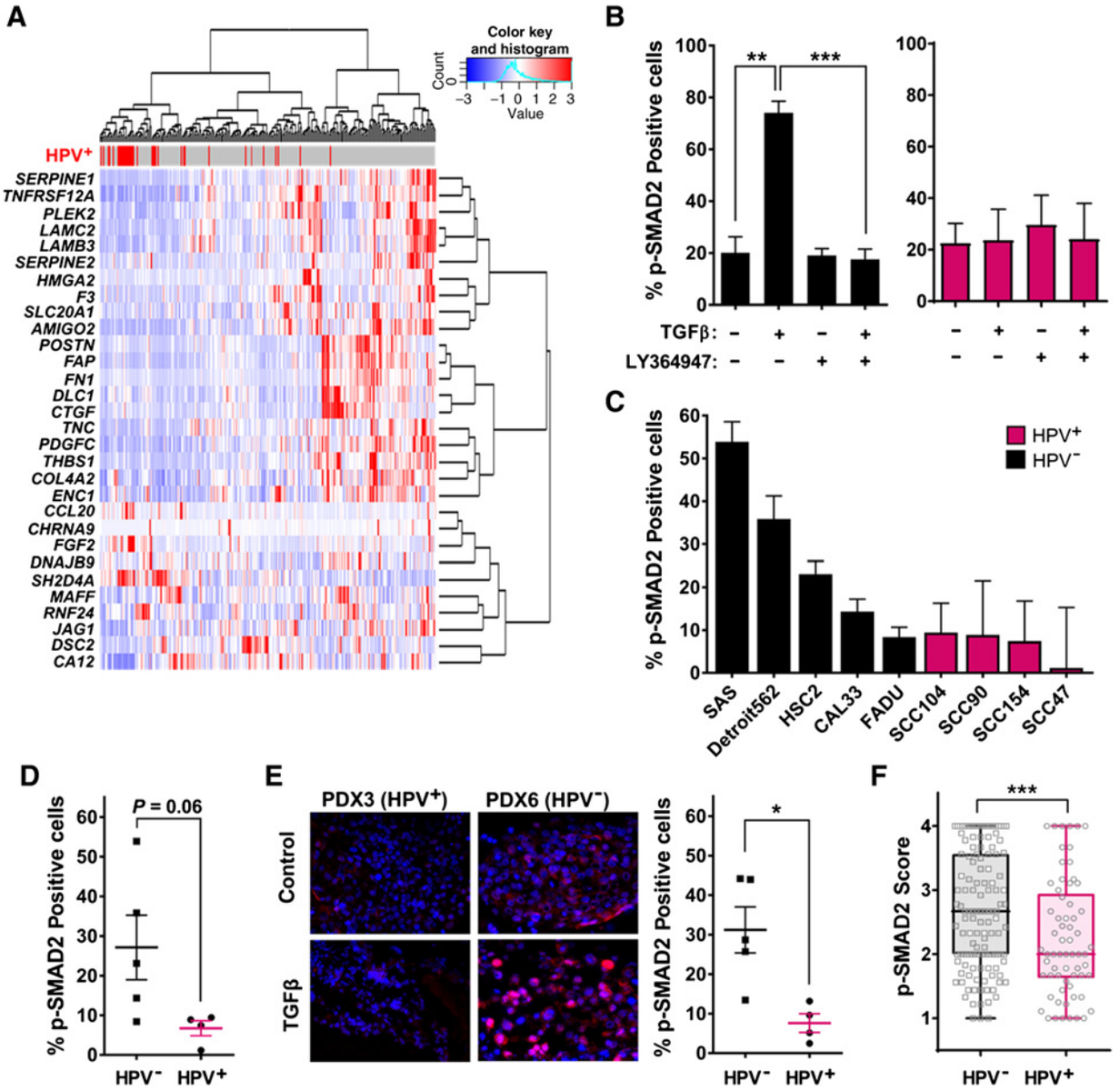

Figure 1.

TGFβ signaling is defective in HPV-positive (HPV$^+$) HNSCC. **A,** Clustering of 243 HPV-negative (HPV$^-$) and 36 HPV$^+$ HNSCC from TCGA using a gene-set signature upregulated by TGFβ signaling. **B,** Percentage of p-SMAD2–positive cells after treatment with TGFβ or TβRI inhibitor LY364947 for a representative HPV$^-$ cell line, SAS (black), and a HPV$^+$ cell line, SCC47 (red). Two-tailed Student *t* test; **, $P < 0.01$; *, $P < 0.005$. **C,** The percentage of p-SMAD2–positive cells following TGFβ treatment of HPV$^-$ cell lines (black) and HPV$^+$ cell lines (red). **D,** Data from panel C grouped according to their HPV status. **E,** Representative images of p-SMAD2 immunostaining of HNSCC PDX (left). The percentage of p-SMAD2–positive cells induced by TGFβ in HPV$^-$ (black) and HPV$^+$ (red) PDX (right). **F,** Distribution of p-SMAD2 scores as described in methods for 130 HPV$^-$ and 65 HPV$^+$ HNSCC. **D–F,** Mann–Whitney *U* test; *, $P < 0.05$; ***, $P < 0.005$.

of p-SMAD2 in a human HNSCC tissue microarray consisting of 194 evaluable cases (Supplementary Fig. S1E; ref. 27). HPV-positive cancers exhibited significantly lower p-SMAD2 levels than did HPV-negative cancers ($P = 0.002$; Fig. 1F). Levels of p-SMAD2 in normal epithelium were not affected by the HPV status of the adjacent cancer (Supplementary Fig. S1F). Together, these analyses of TCGA, cell lines, PDX explants, and tumor specimens provide comprehensive and compelling evidence that TGFβ signaling is significantly compromised in human HPV-positive HNSCC.

Impaired TGFβ signaling associates with better response to radiation and chemotherapy

Our prior work showed that inhibiting TGFβ signaling with LY364947 increased the radiosensitivity of breast, brain, and lung cancer cell lines (16, 18, 20). A short-term assay that reflects both cell-cycle delay and cell kill by measuring cell number 5 days after exposure to 2 Gy (24) showed that HPV-positive HNSCC cell lines significantly more sensitive to radiation than HPV-negative HNSCC cell lines ($P = 0.02$;

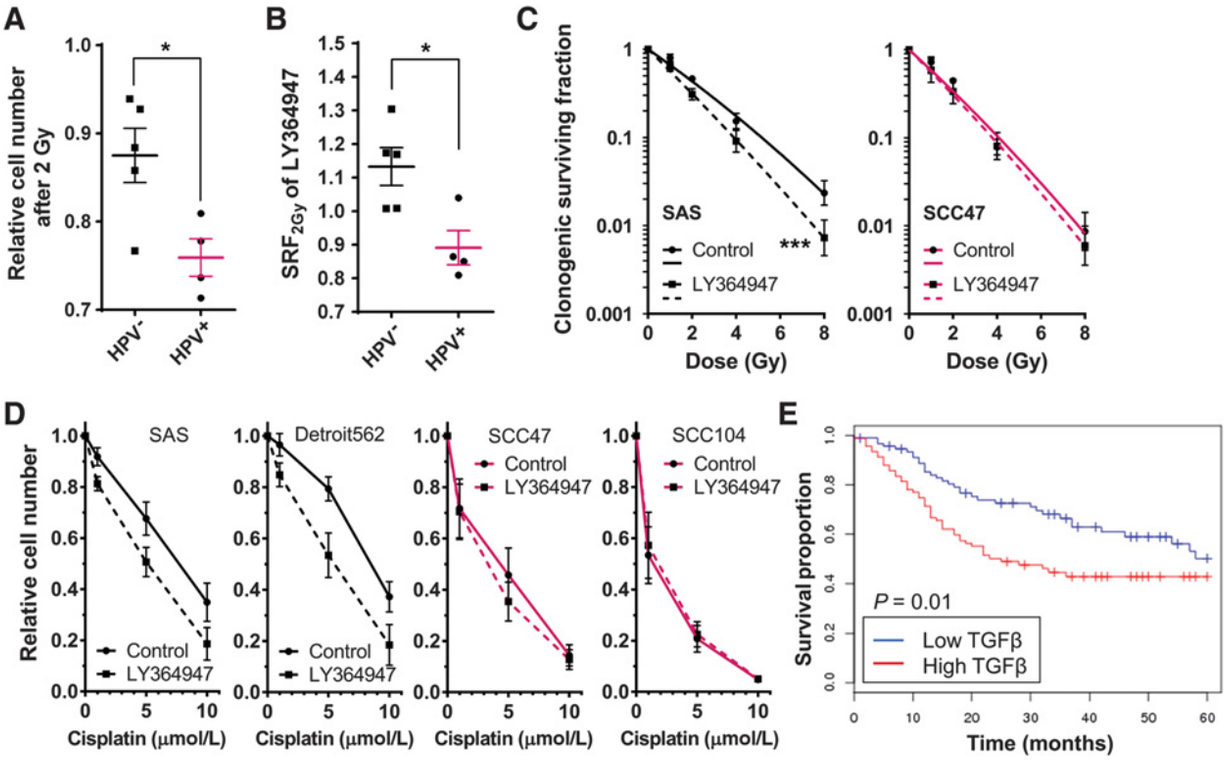

Figure 2.

HNSCC sensitivity to IR or cisplatin correlates with TGFβ signaling status. **A,** Relative cell number after irradiation (2 Gy) measured by a 5-day cell viability assay. HPV^- (black), HPV^+ (red). Two-tailed Mann–Whitney *U* test; *, $P < 0.05$. **B,** SRF_{2Gy} of TβRI inhibitor, LY364947, measured on the HNSCC cell lines. Two-tailed Mann–Whitney *U* test; *, $P < 0.05$. **C,** Surviving fractions and fitted curves from clonogenic assay on HPV^-, SAS or HPV^+, SCC47 cell lines treated with or without TβRI inhibitor LY364947. Statistical difference between survival curves was determined by *F* test; ***, $P < 0.005$. **D,** Relative cell number after cisplatin treatments compared with sham-treated control measured in a 5-day cell proliferation assay. **E,** Kaplan–Meier survival analyses of patients with HNSCC from TCGA with top (i.e., high TGFβ; red) or bottom one-third (i.e., low TGFβ; blue) expression level scores for TGFβ-upregulated genes in Supplementary Fig. S1A. Log-rank test, $P = 0.01$.

Fig. 2A). We then determined radiosensitivity using the response ratio at 2 Gy (SRF_{2Gy}) as reported previously (24). Inhibition of TGFβ signaling using LY364947 radiosensitized all HPV-negative cell lines (i.e., $SRF_{2Gy} > 1$), whereas only one (SCC154) of four HPV-positive cell lines was radiosensitized. As a group, LY364947 treatment significantly increased radiosensitivity of HPV-negative cell lines compared with HPV-positive HNSCC cell lines ($P < 0.05$; Fig. 2B). Notably, the degree of TGFβ responsiveness measured by p-SMAD2 and radiosensitivity measured by SRF_{2Gy} were significantly correlated ($P = 0.04$; Supplementary Fig. S2A).

We confirmed radiation sensitivity by classic clonogenic assay. LY364947 also significantly increased radiosensitivity of the HPV-negative cell line SAS, but did not affect the radiosensitivity of HPV-positive cell line SCC47. Note that SCC47 displayed higher intrinsic radiosensitivity compared with SAS (Fig. 2C). The response to TGFβ inhibition by LY364947 was confirmed by employing two other drugs currently in cancer clinical trials to inhibit TGFβ signaling: a TβRI inhibitor, LY2157299 (Galunisertib), and TGFβ pan-neutralizing antibody, GC1008 (Fresolimumab). Both drugs radiosensitized HPV-negative SAS cells, but neither inhibitor increased radiosensitivity of HPV-positive cell line SCC47 (Supplementary Fig. S2B and S2C). TGFβ inhibition by LY364947 also sensitized HPV-negative cancer cells to cisplatin, but not HPV-positive cells, which were intrinsically more sensitive to cisplatin (Fig. 2D). Moreover, HPV-negative cells exposed to cisplatin in combination with IR were further sensitized by treatment with LY364947 (Supplementary Fig. S2D). The increased cytotoxic response of HNSCC cells in which TGFβ signaling is impaired should improve patient outcomes. Consistent with this, survival of patients in the TCGA cohort whose cancers exhibit low TGFβ activity was significantly better (Fig. 2E).

MiR-182 mechanism by which loss of TGFβ signaling in HPV-positive HNSCC impairs DDR

Our prior work showed that *Tgfb1* genetic deletion impedes ATM autophosphorylation and phosphorylation of its target histone H2AX (γH2AX) upon DNA damage (12, 13). We hypothesized that defective TGFβ signaling in HPV-positive HNSCC would phenocopy *Tgfb1* genetic deletion. We assessed frequency of IR-induced γH2AX foci as a function of LY364947, which did not change cell-cycle distribution in either irradiated or control cells (Supplementary Fig. S3A), nor did HPV status associate with significant difference in proliferation of PDX tissues (Supplementary Fig. S3B). Pretreatment with TβRI inhibitor greatly reduced γH2AX foci formation in irradiated

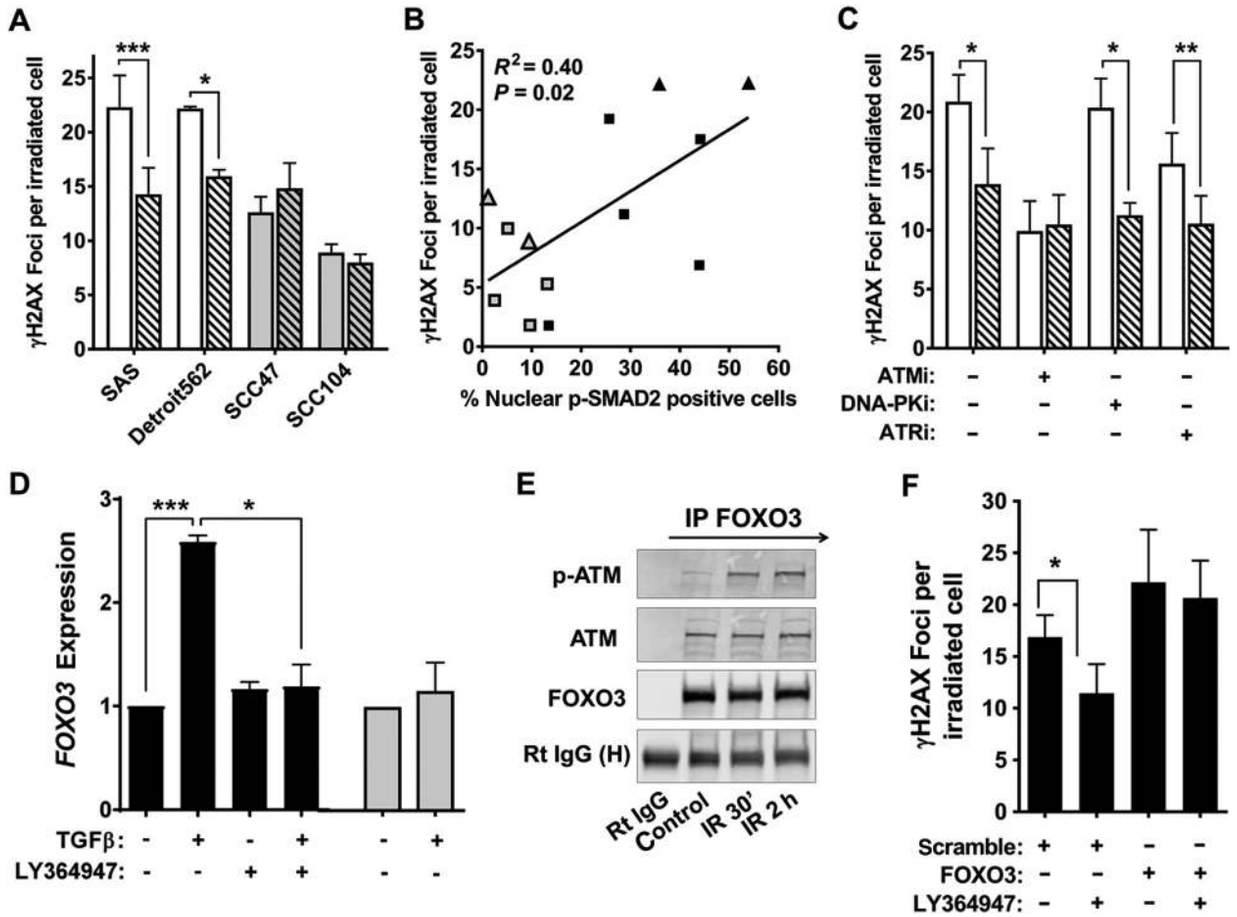

Figure 3.

Impaired TGFβ signaling compromises DNA damage recognition through FOXO3 interaction with ATM. **A,** Number of γH2AX foci per irradiated (2 Gy) HPV$^-$ cell lines (white) and HPV$^+$ cell lines (grey) at 30 minutes post irradiation pretreated with (hatched) or without (open) TβRI inhibitor LY364947. **B,** Correlation of percent nuclear p-SMAD2 positive cells following TGFβ treatment (from Fig. 1C and E) with γH2AX foci (from **A** and Supplementary Fig. S3C) of HPV$^+$ (grey) and negative (black) cell lines (triangles) and PDX (squares). Linear regression analysis was used to calculate *P* value and R^2. **C,** Number of γH2AX foci per cell of irradiated (2 Gy) SAS cells treated with inhibitors against ATM (ATMi, KU55933), DNA-PK (DNA-PKi, KU57788), or ATR (ATRi, AZD6738) with or without LY364947. **D,** Levels of *FOXO3* by qRT PCR in HPV$^-$ SAS (black) and HPV$^+$ SCC47 cell lines (grey) treated with or without TGFβ, TβRI inhibitor LY364947, or combination of both. **E,** Immunoprecipitation (IP) of FOXO3 in sham or irradiated (5 Gy) SAS cells and immunoblotted to detect for p-ATM and ATM. Control rabbit (Rt) IgG was used for sham-IP. Samples were also assayed for heavy chain of Rt IgG (H) as loading control. **F,** Number of γH2AX foci per irradiated (2 Gy) cell at 30 minutes post irradiation pretreated with or without LY364947. SAS cells at 2 days after transfection with FOXO3 expressing or scrambled plasmids were used. Two-tailed Student *t* test; *, $P < 0.05$; **, $P < 0.01$; ***, $P < 0.005$.

HPV-negative cell lines but did not alter γH2AX foci frequency in HPV-positive cell lines (Fig. 3A). Note that the level of IR-induced γH2AX foci of HPV-positive cell lines approximated that following TGFβ inhibition in HPV-negative cell lines. Similarly, fewer IR-induced γH2AX foci were evident in PDX from HPV-positive HNSCC compared with HPV-negative HNSCC, in which LY364947 decreased the number of γH2AX foci (Supplementary Fig. S3C). The degree of TGFβ responsiveness measured by p-SMAD2 correlated with γH2AX foci per irradiated cell across HNSCC specimens and cell lines (Fig. 3B).

Because histone H2AX can be phosphorylated by ATM, ataxia telangiectasia, and Rad3-related (ATR), or DNA-dependent protein kinase (DNA-PK), we tested the contribution of these proteins using specific kinase inhibitors of each (Fig. 3C). Pretreatment with LY364947 further reduced IR-induced γH2AX foci on cells treated with DNA-PK or ATR inhibitor (KU57788 and AZD6738, respectively) but not in cells treated with ATM inhibitor (KU55933), consistent with our conclusion (13) that TGFβ signaling is necessary for ATM kinase activity (Supplementary Fig. S3D).

The mechanism by which TGFβ affects ATM kinase activity has not been identified. Here, we investigated FOXO3 (forkhead box protein O3) because it is required for ATM autophosphorylation (35) and *FOXO3* is targeted by miR-182, which we have shown is regulated by TGFβ (15). *BRCA1* is also a target of miR-182 (15, 36). Consistent with our prior studies, *BRCA1* expression is TGFβ regulated in an HPV-negative cell line but not an HPV-positive cell line (Supplementary Fig. S4A and S4B). Consistent with this, TGFβ increased the expression of *FOXO3* mRNA in a HPV-negative SAS cell line and TGFβ

inhibition with LY364947 blocked this increase, although *FOXO3* expression was unaffected by TGFβ in the HPV-positive cell line SCC47 (Fig. 3D). We confirmed that both ATM and p-ATM were pulled down with FOXO3 immunoprecipitated from extracts of the HPV-negative SAS cell line (Fig. 3E). To test whether FOXO3 was the missing link between TGFβ and ATM kinase, we then overexpressed *FOXO3* in SAS cells (Supplementary Fig. S4C), which abrogated the effect of LY364947 on IR-induced γH2AX foci formation (Fig. 3F). These data suggest that TGFβ regulation of FOXO3 is critical for its effect on ATM kinase activity.

Consistent with TGFβ regulation of miR-182, HPV-positive cell lines exhibited higher levels of miR-182 compared with HPV-negative cell lines (Fig. 4A). TGFβ suppressed miR-182 in a HPV-negative cell line but not a HPV-positive cell line (Fig. 4B). TGFβ-responsive HPV-negative SAS cells were transfected with miR-182 mimic, anti–miR-182, or scrambled controls. Cell-cycle distribution was not affected by modulating miR-182 expression (Supplementary Fig. S4D) as published previously (36), and manipulation of miR-182 did not affect TGFβ induction of p-SMAD2 (Supplementary Fig. S4E). MiR-182 mimic suppressed *FOXO3* and *BRCA1*, whereas anti–miR-182 increased both (Fig. 4C; Supplementary Fig. S4F). Cells transfected with anti–miR-182 and treated with LY364947 did not repress FOXO3 (Fig. 4D) or BRCA1 (Supplementary Fig. S4G). Because TGFβ control of miR-182 regulated FOXO3, we then examined whether functional DDR could be restored by inhibiting miR-182. Antagonizing miR-182 when TGFβ signaling was inhibited by LY364947 restored IR-induced phosphorylation of ATM (Fig. 4E; Supplementary Fig. S5A) and γH2AX foci formation (Fig. 4F). Moreover, LY364947 radiosensitization of SAS cells was eliminated in cells expressing anti–miR-182 (Fig. 4G; Supplementary Fig. S5B).

Of the HPV-negative HNSCC cell lines, *SMAD4*-mutated CAL33 was not radiosensitized by LY364957 (Supplementary Fig. S5C). Consistent with this, SMAD4 protein was completely absent in Cal33 but was also reduced in HPV-positive cell lines (Supplementary Fig. S5D). TGFβ did not suppress miR-182 in CAL33 (Supplementary Fig. S5E). To test the hypothesis that

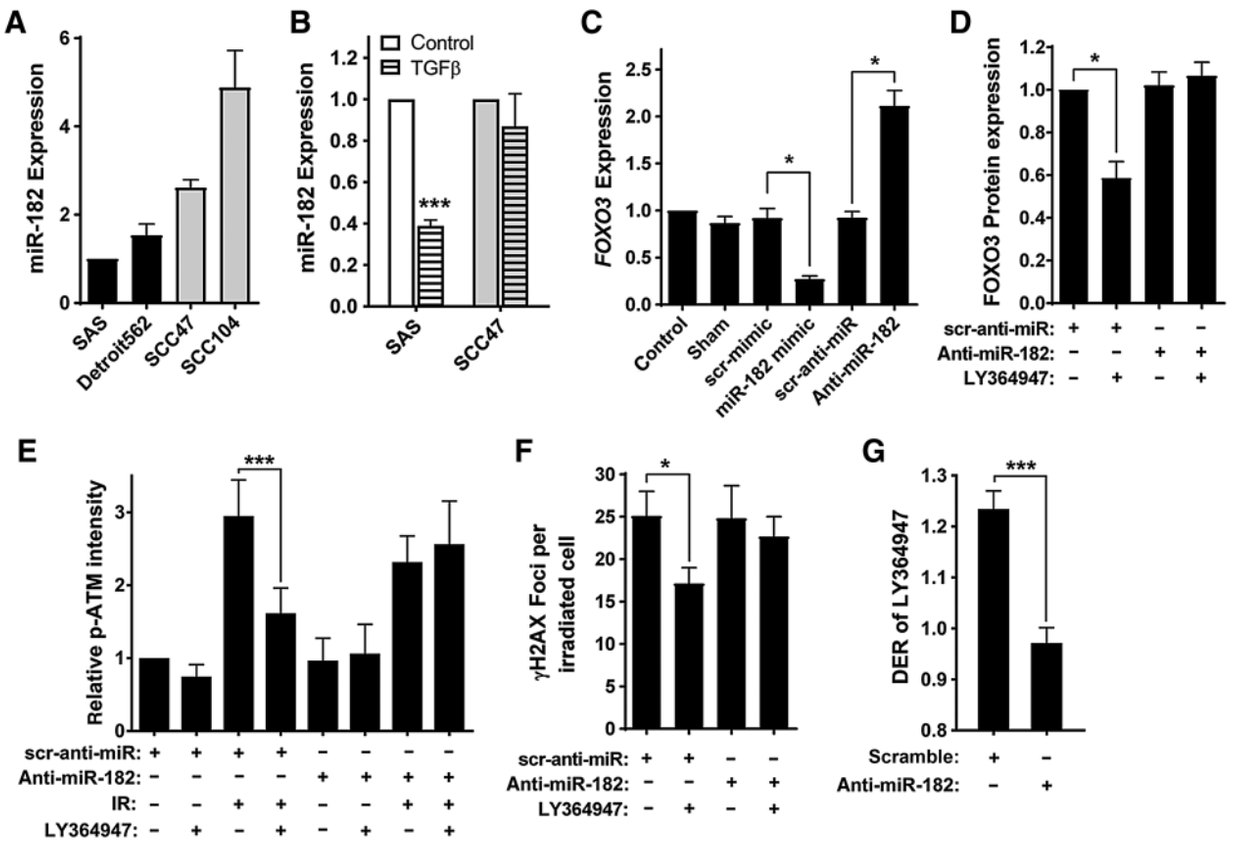

Figure 4.

TGFβ controls DDR through miR-182. **A,** qRT-PCR analyses of miR-182 in HPV$^-$ (black) and HPV$^+$ cell lines (grey). **B,** miR-182 expression in cells treated with (hatched) or without (open) TGFβ. **C,** *FOXO3* mRNA levels in SAS cells transfected with miR-182 mimic, anti-miR-182, or scrambled RNA for 2 days. **D,** Quantified protein expression of FOXO3 with normalization to β-actin. SAS cells were transfected with scramble or anti–miR-182, and treated with or without TβRI inhibitor LY364947. **E,** Quantification of p-ATM protein bands, normalized to total ATM and β-actin, are shown as relative p-ATM intensities. SAS cells were transfected with scrambled RNA or anti–miR-182 and irradiated (5 Gy) with or without LY364947. **F,** γH2AX foci per cell in irradiated (2 Gy) SAS cells transfected with scrambled or anti–miR-182 at 30 minutes post irradiation. **G,** Dose enhancement ratio (DER) of LY364947 measured by clonogenic survival assay of SAS cells transfected with scrambled RNA or anti–miR-182. Two-tailed Student *t* test; *, $P < 0.05$; ***, $P < 0.005$.

TGFβ suppression of miR-182 requires SMAD4, we knocked down SMAD4 by shRNA in SAS cells (Supplementary Fig. S5F). Doing so increased miR-182 expression (Supplementary Fig. S5G) and eliminated the effect of LY364957 on the radiation response measured by SRF_{2Gy} (Supplementary Fig. S5H). We next examined the relationship between SMAD4 mutations and response to cisplatin using the data in the Sanger database. Consistent with loss of TGFβ signaling increasing cisplatin sensitivity in HPV-positive cell lines (Fig. 2D); cell lines in which SMAD4 was suppressed were significantly more sensitive to cisplatin ($P < 0.005$; Supplementary Fig. S5I). Together these data led us to conclude that SMAD4-dependent suppression of miR-182 is the lynchpin by which TGFβ regulates DDR.

Compromised TGFβ signaling impairs HRR proficiency

HRR repairs double strand breaks (DSB) in S and G2 phases when a homologous template is available, during which strand invasion is mediated by recombinase, RAD51, which binds to single-stranded DNA at the processed DSB (37). HRR is compromised in *SMAD4* mutant HNSSC (10). RAD51 foci formation is considered to be a specific marker for execution of HRR. To test whether the loss of TGFβ signaling impeded HRR, we used immunostaining to detect RAD51 foci at its peak time (5–6 hours) in irradiated cell lines and PDX tumor explants. TβRI inhibition decreased RAD51 foci formation after IR in HPV-negative SAS cell line but had no effect in HPV-positive SCC47 cell line (Fig. 5A). Notably, antagonizing miR-182 in the HPV-negative SAS cell line also blocked the effect of TGFβ inhibition on RAD51 foci formation, consistent with HRR restoration (Supplementary Fig. S6A). TβRI inhibition significantly reduced RAD51 foci formation in HPV-negative PDX explants and approached the low levels in HPV-positive explants (Fig. 5B). To validate TGFβ impact on HRR, we established HPV-negative SAS cells expressing constructs in which green fluorescent protein (GFP) is expressed if HRR occurs following an endonuclease-generated DSB (38). The

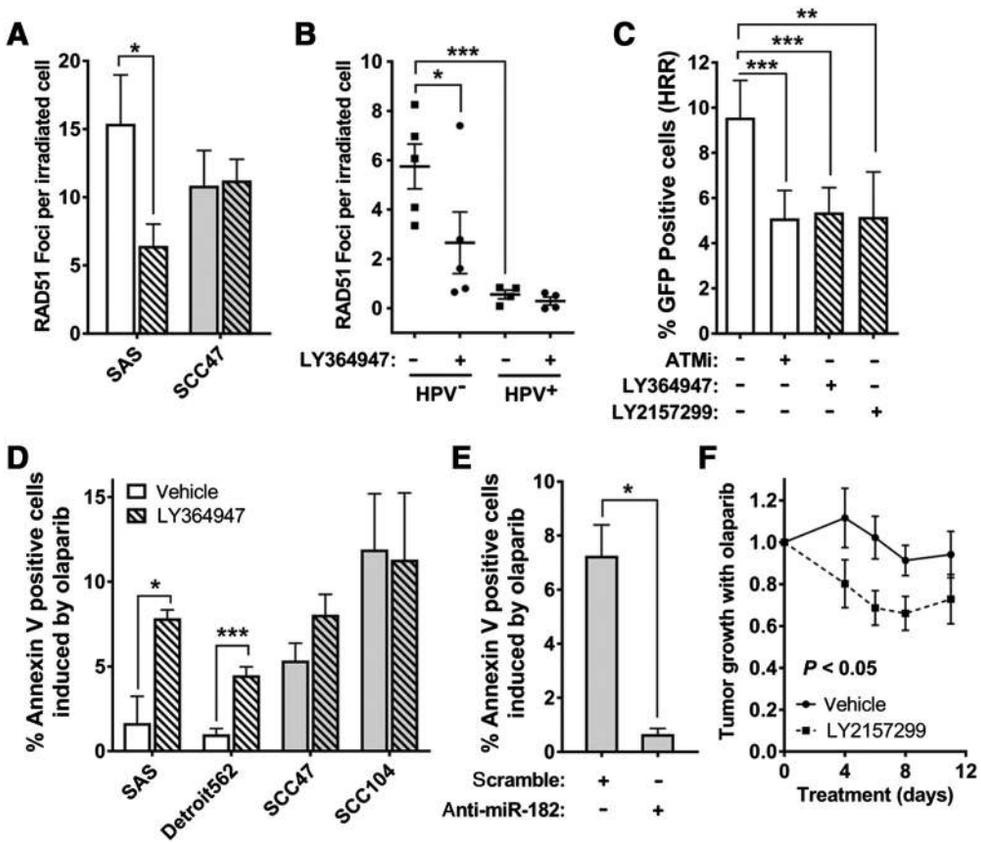

Figure 5.

Decreased TGFβ signaling impedes DNA repair through HRR. **A,** Number of RAD51 foci per cell at 6 hours post irradiation (4 Gy) in HPV^- (white) SAS cell line and HPV^+ (grey) SCC47 cell line pretreated with (hatched) or without (open) LY364947. **B,** RAD51 foci per cell of irradiated (4 Gy) PDX samples grouped according to HPV status and LY364947 treatments. **C,** Flow cytometry analyses of I-SceI-HRR reporter SAS cell clone treated with TβRI inhibitors, LY364947 and LY2157299, or ATM inhibitor (ATMi), KU55933. Percentage of GFP-positive cells after indicated treatments on I-SceI-HRR reporter cells. **D,** Percentage of annexin V positive cells induced by olaparib with (hatched) or without (open) LY364947 in HPV^- (white) and HPV^+ cell lines (grey). **E,** Percentage of annexin V–positive cells induced by olaparib in HPV^+ SCC47 cells transfected with scrambled or anti–miR-182. **F,** Tumor growth rate of SAS xenografts treated with olaparib, with or without LY2157299, were plotted against days after the first treatment of drugs; control tumor volumes without olaparib treatment were normalized to one; Two-way ANOVA; $P < 0.05$. Two-tailed Student t test; *, $P < 0.05$; **, $P < 0.05$; ***, $P < 0.005$.

frequency of HRR was decreased by approximately 50% when TβRI kinase was inhibited by either of two small molecules (Fig. 5C), which was comparable with that observed following ATM inhibition by KU55933. These data indicate that HRR is compromised by inhibition of TGFβ signaling and is defective in HPV-positive HNSCC.

HRR-deficient cells are more sensitive to inhibition of PARP1 due to synthetic lethality, the paradigmatic example of which is that between *BRCA1/2* loss-of-function and sensitivity to PARP inhibition (39). A dose response in the HPV-negative SAS cell line showed that TGFβ inhibition increased sensitivity to olaparib by fourfold (Supplementary Fig. S6B). Using annexin-V staining for apoptosis induced in olaparib-treated cell lines, we found that HPV-positive cell lines were more sensitive to olaparib compared with HPV-negative cells. However, HPV-negative cells pretreated with LY364957 were sensitized to olaparib (Fig. 5D). SMAD4 knockdown in SAS cells also increased sensitivity to PARP1 inhibition (Supplementary Fig. S6C and S6D). Moreover, SMAD4 mutant HNSCC cell lines in the Sanger database showed greater sensitivity to olaparib than those in which SMAD4 is wild-type (Supplementary Fig. S6E ; ref. 40). Importantly, the pronounced sensitivity in HPV-positive SCC47 cells to PARP inhibition was rescued by transfection of the miR-182 antagonist (Fig. 5E). Olaparib sensitivity is of significant interest clinically and these data suggest a nonresponsive cancer could be sensitized by inhibiting TGFβ signaling. To test this, we established SAS xenografts and treated them with olaparib with and without TGFβ small-molecule inhibitor, LY2157299. As expected, olaparib treatment of TGFβ competent SAS had little effect on tumor growth over the 12-day treatment. However, simultaneous treatment with LY2157299 elicited significant tumor growth inhibition (Fig. 5F).

Loss of TGFβ responsiveness shifts DNA repair to alt-EJ

Alt-EJ pathways are thought to compete, albeit poorly, with HRR for DSB repair in S phase, and back up repair when either HRR or NHEJ is compromised (41). To evaluate the repair from alt-EJ, we established a SAS cell clone with a GFP reporter construct that detects alt-EJ events resulting from I-SceI endonuclease-induced DSB (30). Two different inhibitors of TGFβ signaling significantly increased the frequency of alt-EJ events (Fig. 6A). In contrast, a specific PARP1 inhibitor, AG14361, reduced the frequency of alt-EJ events because PARP is necessary for alt-EJ. Thus, HNSCC with deficient TGFβ signaling may use alt-EJ more frequently. Indeed, analysis of HNSCC TCGA indicates that HPV-positive cancers exhibit significantly greater expression of PARP1 and POLQ, both of which are critical components in alt-EJ (Supplementary Fig. S7A).

Alt-EJ is both less efficient and more error prone than HRR, which leads to more residual damage and cell death. We created POLQ isogenic cell pair in HPV-negative cell line SAS to investigate roles of POLQ in TGFβ repressed alt-EJ (Supplementary Fig. S7B). The low frequency of alt-EJ events in control cells was further reduced in POLQ-deleted cells, and the effect of TGFβ inhibition was completely eliminated (Fig. 6B). Alt-EJ promotes genomic instability and contributes to chromosome aberrations, especially translocations (41). Consistent with upregulated alt-EJ after TGFβ inhibition, TGFβ inhibition increased chromosome aberrations (CAs) in irradiated HPV-negative SAS cells but CA were not significantly affected by TGFβ inhibition in cells with POLQ knockdown (Supplementary Fig. S7C). The analysis of neutral comet tail moments reflects DSB that are unrepaired or DNA fragmentation from cells undergoing apoptosis, either of which demonstrates poor execution of the DDR. Irradiated POLQ-depleted cells and control cells displayed similar tail moments in a neutral comet assay. However when TGFβ signaling was blocked prior to irradiation, tail moment was significantly greater in POLQ-depleted cells (Fig. 6C). This differential was evident by clonogenic assay, in which survival of POLQ-depleted cells was significantly decreased by TGFβ inhibition or irradiation (Fig. 6D). Notably, radiosensitivity is greatest when both TGFβ signaling and POLQ function are inactive. These data led us to conclude that cells with defective TGFβ signaling have a specific requirement for POLQ, consistent with a shift to alt-EJ repair.

To validate the relevance of these *in vitro* studies to human HNSCC, we used explants of 10 HNSCC (Supplementary Fig. S7D). Immunostaining of p-SMAD2 indicative of endogenous TGFβ signaling varied in these HNSCC specimens (Supplementary Fig. S7E), but the average of HPV-positive specimens was significantly lower than that of HPV-negative specimens (Supplementary Fig. S7F). To measure DNA repair proficiency, we used frequency of P53-binding protein 1 (53BP1) foci after irradiation, whose persistence indicate poor DSB repair (42). Explants were treated with and without TβR1 kinase inhibitor LY2157299 prior to irradiation and 53BP1 nuclear foci were measured at 5 hours postradiation. HPV-negative HNSCC showed few (∼2) 53BP1 foci, consistent with repair proficiency, whereas HPV-positive HNSCC exhibited more than twice as many 53BP1 residual foci, indicative of poor repair (Fig. 6E). As a group, HPV-negative HNSCC explants in which TGFβ signaling was inhibited showed significantly more persistent 53BP1 foci, which approached the baseline levels of HPV-positive explants that were unresponsive TGFβ inhibition (Fig. 6F). To confirm this as an evidence of unrepaired DNA damage, we employed the neutral comet assay to detect residual DSB in primary HNSCC cancers irradiated as explants. Irradiated HPV-positive HNSCC explains showed significantly greater residual DNA damage upon PARP1 inhibition compared with HPV-negative samples (Fig. 6G). We hypothesized that the use of TGFβ inhibitors in HPV-negative specimens would replicate the consequences of HPV infection on PARP sensitivity. Notably, HPV-negative explants exhibited minimal response to PARP inhibition alone but residual DNA damage significantly increased when combined with LY2157299, which also increased unrepaired DSB following exposure to radiation. Moreover, the triple combination of radiation, PARP inhibition, and LY2157299 resulted in more residual damage (i.e., less repair) than either double combination (Fig. 6H). Thus, loss of TGFβ signaling in HPV-positive cancers compromises DNA repair and increases vulnerability to cytotoxic therapy and, which can be recapitulated in HPV-negative cancer by pharmaceutical inhibition of TGFβ signaling.

Discussion

Although the greater sensitivity of HPV-positive HNSCC to cytotoxic therapy is well documented, our studies provide compelling evidence, that the basis for this differential is abrogation of TGFβ signaling. Loss of TGFβ signaling releases suppression of miR-182 that targets both BRCA1 and FOXO3, the latter is necessary for ATM kinase activity, for degradation. As both BRCA1 and ATM are essential for HRR, their loss

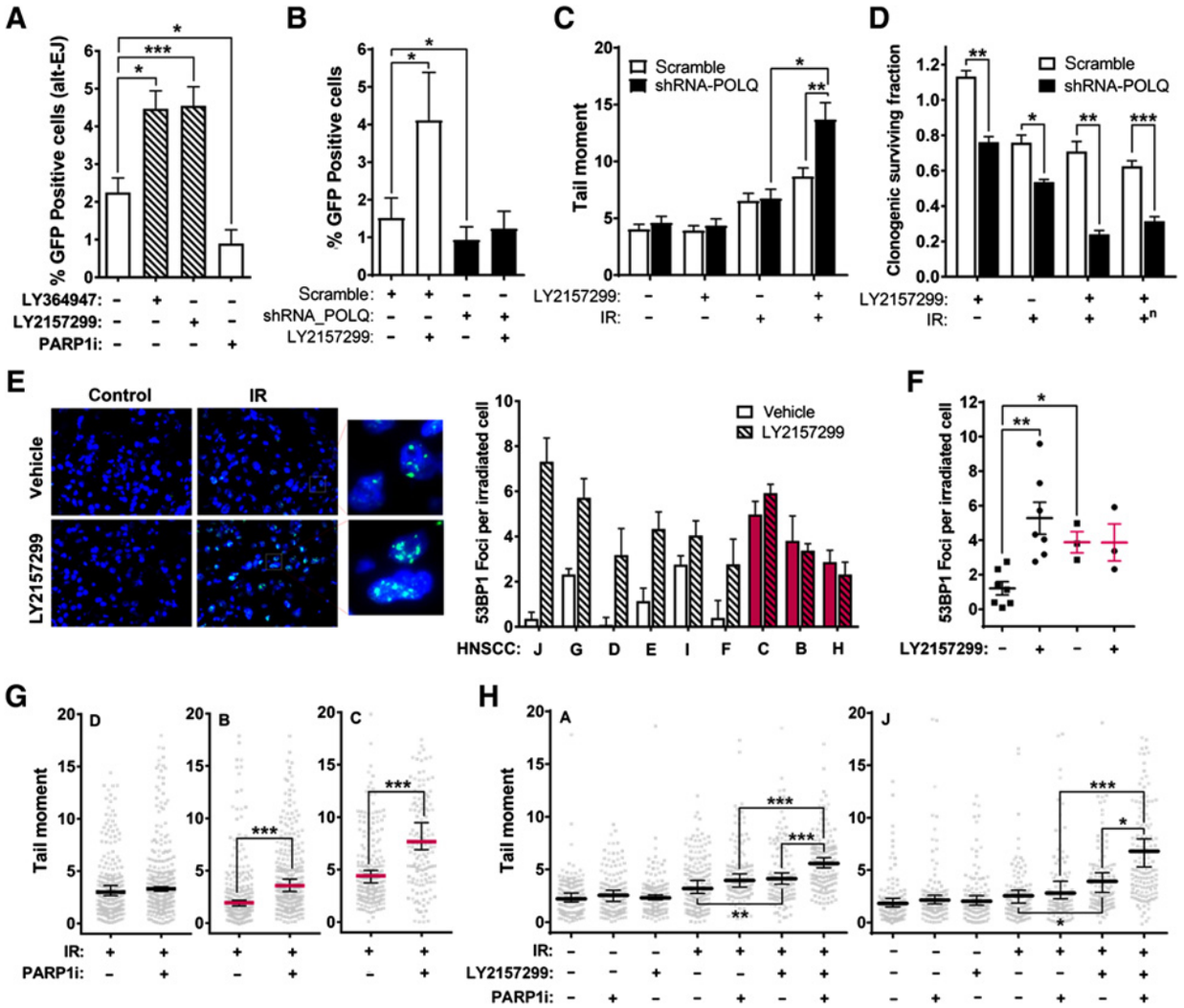

Figure 6.

Loss of TGFβ signaling increases reliance on alt-EJ. **A,** Percentage of GFP-positive cells from I-SceI-alt-EJ reporter cells treated with TβRI inhibitors (LY364947 or LY2157299 at 0.4 μmol/L) or PARP1 inhibitor AG14361 (PARP1i) at 1 μmol/L. **B,** Percentage of GFP-positive cells from I-SceI-alt-EJ reporter cells transfected with POLQ or scrambled shRNA. **C,** Olive tail moments 5 hours after 0 or 10 Gy irradiation of SAS cells transfected with POLQ or scrambled shRNA treated with LY2157299 or vehicle control for 24 hours. **D,** Clonogenic surviving fractions of isogenic SAS cell pair transfected with shPOLQ or scrambled RNA exposed to 2 Gy radiation with or without LY2157299. Superscript "n" indicates that difference in LY2157299 alone effects has been normalized. **E,** Representative images of 53BP1 foci in HPV$^-$ primary HNSCC "G" (see Supplementary Fig. S7D; left). Number of 53BP1 foci per cell in irradiated (4 Gy) HPV$^-$ (white) and HPV$^+$ (red) HNSCC specimens pretreated with (hatched) or without (open) LY2157299 at 5 hours post irradiation (right). **F,** Data from HNSCC specimens in **E** grouped according to HPV status and LY2157299 treatments. **A–F,** Two-tailed Student *t* test; *, $P < 0.05$; **, $P < 0.05$; ***, $P < 0.005$. **G,** Olive tail moments of irradiated (10 Gy, 5 hours) HPV$^-$ (black) or HPV$^+$ (red) HNSCC (HNSCC_ "D," "B," and "C") treated with or without PARP1i AG14361. Median values are shown with 95% confidence intervals. **H,** Olive tail moments of HPV$^-$ cells (HNSCC_ "A" and "J") treated with or without IR, TβRI inhibitor LY2157299, AG14361, or combinations. **G** and **H,** Mann–Whitney *U* test; *, $P < 0.05$; **, $P < 0.01$; ***, $P < 0.005$.

increases sensitivity to radiation, cisplatin, and PARP inhibition. Unexpectedly, the penultimate mechanism by which HPV sensitizes HNSCC to cytotoxic therapy is a shift to alt-EJ repair, which is more error prone and creates vulnerability by relying on novel targets, such as POLQ, that could be exploited clinically (43).

Control of the DDR is an underappreciated facet of TGFβ biology (44). The current studies demonstrate that failure of TGFβ signaling from HPV infection or pharmaceutical inhibition redirects DDR pathway choice. Both classical pathways for DSB repair, that is, NHEJ and HRR, are affected by TGFβ signaling. TGFβ positively regulates ligase IV (14), which is a critical player in NHEJ. Our studies show that HRR is specifically decreased upon TGFβ inhibition by either HPV abrogation or pharmaceutical blockade of receptor-mediated TGFβ signaling. We identified TGFβ suppression of miR-182 as the key link between ATM and BRCA1. BRCA1 affects HRR through two major steps: facilitating the processing and resection of

DNA broken ends, and binding of RAD51 to ssDNA. ATM is not only needed for initiation but also for completion of HRR (45). Indeed, ATM defects are also synthetic lethal with PARP inhibition (46). In addition, failure of ATM kinase impairs DSB recognition, which is often assessed by analyzing γH2AX, itself a substrate for ATM phosphorylation (13).

TGFβ inhibition sensitizes brain, breast, and lung cancer cells to radiation-induced clonogenic cell death and improves tumor control in preclinical tumors (18, 20, 22, 25). Blockade of TGFβ signaling also augments the response of brain tumor models to chemoradiation (19, 21). Teicher and colleagues demonstrated that TGFβ activity contributes to drug resistance and hinders response to chemotherapy in liver and colon cancer preclinical models (47). Pharmacologic approaches to block TGFβ signaling include mAbs, antisense oligonucleotides, and small-molecule inhibitors (17). The consensus of these studies and ongoing trials is that TGFβ inhibition can be achieved safely, but the major questions remain as to which patients will benefit, and which of TGFβ's pleiotropic actions contribute to therapeutic outcome.

Abrogation of TGFβ signaling is an extremely frequent event in HNSCC. The frequency of *SMAD4* deletion in HPV-negative HNSCC led Wang and colleagues to engineer conditional deletion of Smad4 that resulted in a murine model of spontaneous HNSCC (10). Consistent with our studies, these tumors are characterized by genomic instability and decreased HRR (10). HPV infection is functionally equivalent to *SMAD4* deletion because oncogenes E5, E6, and E7 essentially abrogate TGFβ signaling. Viral protein E5 decreases phosphorylation of SMAD2 and nuclear translocation of SMAD4, as well as progressive downregulation of TβRII (48); E6 renders cells resistant to TGFβ-mediated growth control by interacting and degrading TIP-2/GIPC (49), and E7 interacts constitutively with SMAD2, 3, and 4, which significantly impedes SMAD4-mediated transcriptional activity (50). Hence, HPV-positive HNSCC provides an "experiment of nature" that demonstrates the critical role of TGFβ signaling in efficient execution of the DDR. Given the significant survival differential between cancer patients with HPV-positive and HPV-negative, our studies provide strong rationale to treat cancers in which TGFβ signaling is intact with TGFβ blocking pharmaceuticals with the aim to compromise DNA repair and improve outcome from DNA damaging therapy or PARP inhibitors.

There are several limitations of our studies. Radiation sensitivity was determined using a short-term assay rather the gold-standard colony formation assay because not all cell lines formed colonies. Furthermore, we used one HPV-negative cell, SAS, to investigate the mechanism by which miR182 mediates ATM activity through regulating FOXO3 expression, as well as the synergistic effects between TGFβ inhibition and POLQ knock down. It is likely that different molecular contexts could affect the pathway interactions. Further validation of our results in larger panel of cancer cell lines and patient tumor data, perhaps across cancer types, would ascertain if the mechanism is conserved. In addition, the contribution of noncanonical TGFβ signaling could be of potential interest. Nevertheless, the consistency of responses from HPV-positive and -negative PDX, TCGA data, and primary tumor explants provide confidence that the fundamental biology regulated by TGFβ is important to pursue. Our future studies will focus on determining whether prognosis is TGFβ dependent for certain patients, as well as testing our prediction that TGFβ inhibition could synergize with PARP inhibitors.

Disclosure of Potential Conflicts of Interest

M.H. Barcellos-Hoff reports receiving speakers bureau honoraria from Genzyme, Inc. and Genentech, and is a consultant/advisory board member for Telios, Inc. and Varian, Inc. M.A. Pujana reports receiving commercial research grants from Roche Farma. No potential conflicts of interest were disclosed by the other authors.

Authors' Contributions

Conception and design: Q. Liu, H. Martinez-Ruiz, J. Seoane, M.H. Barcellos-Hoff
Development of methodology: Q. Liu, L. Ma, J. Murnane, J. Seoane
Acquisition of data (provided animals, acquired and managed patients, provided facilities, etc.): Q. Liu, T. Jones, H. Martinez-Ruiz, P.K. Ha, I. Cuartas, M. Baumann, A. Linge
Analysis and interpretation of data (e.g., statistical analysis, biostatistics, computational analysis):, Q. Liu, L. Ma, T. Jones, L. Palomero, J. Murnane, J. Seoane, M.H. Barcellos-Hoff
Writing, review, and/or revision of the manuscript: Q. Liu, L. Ma, T. Jones, P.K. Ha, J. Murnane, M. Baumann, A. Linge, M.H. Barcellos-Hoff
Administrative, technical, or material support (i.e., reporting or organizing data, constructing databases): Q. Liu, L. Ma, T. Jones, I. Cuartas
Study supervision: Q. Liu, M.H. Barcellos-Hoff

Acknowledgments

The authors would like to thank Drs. Simon Powell, Henning Willers, George Iliakis, and Alba Gonazlez-Junca for helpful comments, DKTK-ROG, and Dr. Jeremy Stark for reagents, and Mr. William Chou and Ms. Shiva Bolourchi for experimental support. This study was funded by the UCSF Department of Radiation Oncology seed funding and the Wun-Kon Fu Endowed Chair in Radiation Oncology to MHBH.

The costs of publication of this article were defrayed in part by the payment of page charges. This article must therefore be hereby marked *advertisement* in accordance with 18 U.S.C. Section 1734 solely to indicate this fact.

Received April 30, 2018; revised June 15, 2018; accepted August 2, 2018; published first August 7, 2018.

References

1. Marur S, Forastiere AA. Head and neck squamous cell carcinoma: update on epidemiology, diagnosis, and treatment. Mayo Clin Proc 2016;91:386–96.
2. Lohaus F, Linge A, Tinhofer I, Budach V, Gkika E, Stuschke M, et al. Hpv16 DNA status is a strong prognosticator of loco-regional control after post-operative radiochemotherapy of locally advanced oropharyngeal carcinoma: results from a multicentre explorative study of the german cancer consortium radiation oncology group (dktk-rog). Radiother Oncol 2014;113:317–23.
3. Ziemann F, Arenz A, Preising S, Wittekindt C, Klussmann JP, Engenhart-Cabillic R, et al. Increased sensitivity of hpv-positive head and neck cancer cell lines to x-irradiation +/− cisplatin due to decreased expression of e6 and e7 oncoproteins and enhanced apoptosis. Am J Cancer Res 2015; 5:1017–31.
4. Mirghani H, Amen F, Tao Y, Deutsch E, Levy A. Increased radiosensitivity of hpv-positive head and neck cancers: molecular basis and therapeutic perspectives. Cancer Treat Rev 2015;41: 844–52.

5. Weaver AN, Cooper TS, Rodriguez M, Trummell HQ, Bonner JA, Rosenthal EL, et al. DNA double strand break repair defect and sensitivity to poly adp-ribose polymerase (parp) inhibition in human papillomavirus 16-positive head and neck squamous cell carcinoma. Oncotarget 2015;6:26995–7007.
6. Wallace NA, Khanal S, Robinson KL, Wendel SO, Messer JJ, Galloway DA. High-risk alphapapillomavirus oncogenes impair the homologous recombination pathway. J Virol 2017;91 pii: e01084-17. https://www.ncbi.nlm.nih.gov/pubmed/28768872.
7. Ceccaldi R, Rondinelli B, D'Andrea AD. Repair pathway choices and consequences at the double-strand break. Trends Cell Biol 2016;26: 52–64.
8. Perez-Plasencia C, Vazquez-Ortiz G, Lopez-Romero R, Pina-Sanchez P, Moreno J, Salcedo M. Genome wide expression analysis in hpv16 cervical cancer: identification of altered metabolic pathways. Infect Agent Cancer 2007;2:16.
9. Seoane J, Gomis RR. Tgf-beta family signaling in tumor suppression and cancer progression. Cold Spring Harb Perspect Biol 2017;9 pii: a022277https://www.ncbi.nlm.nih.gov/pubmed/28246180.
10. Bornstein S, White R, Malkoski S, Oka M, Han G, Cleaver T, et al. Smad4 loss in mice causes spontaneous head and neck cancer with increased genomic instability and inflammation. J Clin Invest 2009; 119:3408–19.
11. Glick AB, Weinberg WC, Wu IH, Quan W, Yuspa SH. Transforming growth factor beta 1 suppresses genomic instability independent of a g1 arrest, p53, and rb. Cancer Res 1996;56:3645–50.
12. Ewan KB, Henshall-Powell RL, Ravani SA, Pajares MJ, Arteaga CL, Warters RL, et al. Transforming growth factor-b1 mediates cellular response to DNA damage in situ. Cancer Res 2002;62:5627–31.
13. Kirshner J, Jobling MF, Pajares MJ, Ravani SA, Glick A, Lavin M, et al. Inhibition of tgfb1 signaling attenuates atm activity in response to genotoxic stress. Cancer Res 2006;66:10861–68.
14. Kim MR, Lee J, An YS, Jin YB, Park IC, Chung E, et al. Tgfbeta1 protects cells from gamma-ir by enhancing the activity of the nhej repair pathway. Mol Cancer Res 2015;13:319–29.
15. Martinez-Ruiz H, Illa-Bochaca I, Omene C, Hanniford D, Liu Q, Hernando E, et al. A tgfbeta-mir-182-brca1 axis controls the mammary differentiation hierarchy. Sci Signal 2016;9:ra118.
16. Du S, Barcellos-Hoff MH. Biologically augmenting radiation therapy by inhibiting tgfβ actions in carcinomas. Sem Radiat Oncol 2013; 23:242–51.
17. Akhurst RJ, Hata A. Targeting the tgfb signalling pathway in disease. Nat Rev Drug Discov 2012;11:790–811.
18. Bouquet SF, Pal A, Pilones KA, Demaria S, Hann B, Akhurst RJ, et al. Transforming growth factor b1 inhibition increases the radiosensitivity of breast cancer cells *in vitro* and promotes tumor control by radiation *in vivo*. Clin Cancer Res 2011;17:6754–65.
19. Anido J, Saez-Borderias A, Gonzalez-Junca A, Rodon L, Folch G, Carmona MA, et al. Tgf-beta receptor inhibitors target the cd44(high)/id1(high) glioma-initiating cell population in human glioblastoma. Cancer Cell 2010;18:655–68.
20. Hardee ME, Marciscano AE, Medina-Ramirez CM, Zagzag D, Narayana A, Lonning SM, et al. Resistance of glioblastoma-initiating cells to radiation mediated by the tumor microenvironment can be abolished by inhibiting transforming growth factor-β. Cancer Res 2012;72:4119–29.
21. Zhang M, Lahn M, Huber PE. Translating the combination of tgfbeta blockade and radiotherapy into clinical development in glioblastoma. Oncoimmunology 2012;1:943–5.
22. Du S, Bouquet F, Lo C-H, Pellicciotta I, Bolourchi S, Parry R, et al. Attenuation of the DNA damage response by tgfβ inhibitors enhances radiation sensitivity of nsclc cells *in vitro* and *in vivo*. Int J Radiat Oncol Biol Phys 2014;91:91–9.
23. Zhao M, Sano D, Pickering CR, Jasser SA, Henderson YC, Clayman GL, et al. Assembly and initial characterization of a panel of 85 genomically validated cell lines from diverse head and neck tumor sites. Clin Cancer Res 2011;17:7248–64.
24. Liu Q, Wang M, Kern AM, Khaled S, Han J, Yeap BY, et al. Adapting a drug screening platform to discover associations of molecular targeted radiosensitizers with genomic biomarkers. Mol Cancer Res 2015;13: 713–20.
25. Bayin NS, Ma L, Thomas C, Baitalmal R, Sure A, Fansiwala K, et al. Patient-specific screening using high-grade glioma explants to determine potential radiosensitization by a tgf-β small molecule inhibitor. Neoplasia 2016; 18:795–805.
26. Herbert AD, Carr AM, Hoffmann E. Findfoci: a focus detection algorithm with automated parameter training that closely matches human assignments, reduces human inconsistencies and increases speed of analysis. PLoS One 2014;9:e114749.
27. Linge A, Lock S, Gudziol V, Nowak A, Lohaus F, von Neubeck C, et al. Low cancer stem cell marker expression and low hypoxia identify good prognosis subgroups in hpv(-) hnscc after postoperative radiochemotherapy: a multicenter study of the dktk-rog. Clin Cancer Res 2016;22:2639–49.
28. Seoane J, Le HV, Shen L, Anderson SA, Massague J. Integration of smad and forkhead pathways in the control of neuroepithelial and glioblastoma cell proliferation. Cell 2004;117:211–23.
29. Pierce AJ, Johnson RD, Thompson LH, Jasin M. Xrcc3 promotes homology-directed repair of DNA damage in mammalian cells. Genes Dev 1999;13: 2633–8.
30. Bennardo N, Cheng A, Huang N, Stark JM. Alternative-nhej is a mechanistically distinct pathway of mammalian chromosome break repair. PLoS Genet 2008;4:e1000110. https://www.ncbi.nlm.nih.gov/pubmed/18584027.
31. Muraki K, Han L, Miller D, Murnane JP. The role of atm in the deficiency in nonhomologous end-joining near telomeres in a human cancer cell line. PLoS Genet 2013;9:e1003386.
32. Gyori BM, Venkatachalam G, Thiagarajan PS, Hsu D, Clement MV. Opencomet: an automated tool for comet assay image analysis. Redox Biol 2014;2:457–65.
33. The Cancer Genome Atlas Network. Comprehensive genomic characterization of head and neck squamous cell carcinomas. Nature 2015; 517:576–82.
34. Hanzelmann S, Castelo R, Guinney J. Gsva: gene set variation analysis for microarray and rna-seq data. BMC Bioinformatics 2013;14:7.
35. Tsai W-B, Chung YM, Takahashi Y, Xu Z, Hu MCT. Functional interaction between foxo3a and atm regulates DNA damage response. Nat Cell Biol 2008;10:460–7.
36. Moskwa P, Buffa FM, Pan Y, Panchakshari R, Gottipati P, Muschel RJ, et al. Mir-182-mediated downregulation of brca1 impacts DNA repair and sensitivity to parp inhibitors. Mol Cell 2011;41:210–20.
37. Powell SN, Kachnic LA. Roles of brca1 and brca2 in homologous recombination, DNA replication fidelity and the cellular response to ionizing radiation. Oncogene 2003;22:5784–91.
38. Weinstock DM, Nakanishi K, Helgadottir HR, Jasin M. Assaying double-strand break repair pathway choice in mammalian cells using a targeted endonuclease or the rag recombinase. Methods Enzymol 2006; 409:524–40.
39. Farmer H, McCabe N, Lord CJ, Tutt AN, Johnson DA, Richardson TB, et al. Targeting the DNA repair defect in brca mutant cells as a therapeutic strategy. Nature 2005;434:917–21.
40. Garnett MJ, Edelman EJ, Heidorn SJ, Greenman CD, Dastur A, Lau KW, et al. Systematic identification of genomic markers of drug sensitivity in cancer cells. Nature 2012;483:570–5.
41. Iliakis G, Murmann T, Soni A. Alternative end-joining repair pathways are the ultimate backup for abrogated classical non-homologous end-joining and homologous recombination repair: implications for the formation of chromosome translocations. Mutat Res Genet Toxicol Environ Mutagen 2015;793:166–75.
42. Panier S, Boulton SJ. Double-strand break repair: 53bp1 comes into focus. Nat Rev Mol Cell Biol 2014;15:7–18.
43. Higgins GS, Boulton SJ. Beyond parp-poltheta as an anticancer target. Science 2018;359:1217–8.
44. Barcellos-Hoff MH, Cucinotta FA. New tricks for an old fox: impact of tgfbeta on the DNA damage response and genomic stability. Sci Signal 2014;7:re5.
45. Bakr A, Oing C, Kocher S, Borgmann K, Dornreiter I, Petersen C, et al. Involvement of atm in homologous recombination after end resection and rad51 nucleofilament formation. Nucleic Acids Res 2015;43:3154–66.

46. Liu Q, Gheorghiu L, Drumm M, Clayman R, Eidelman A, Wszolek MF, et al. Parp-1 inhibition with or without ionizing radiation confers reactive oxygen species-mediated cytotoxicity preferentially to cancer cells with mutant tp53. Oncogene 2018;37:2793–805.
47. Teicher BA, Maehara Y, Kakeji Y, Ara G, Keyes SR, Wong J, et al. Reversal of *in vivo* drug resistance by the transforming growth factor-beta inhibitor decorin. Int J Cancer 1997;71:49–58.
48. French D, Belleudi F, Mauro MV, Mazzetta F, Raffa S, Fabiano V, et al. Expression of hpv16 e5 down-modulates the tgfbeta signaling pathway. Mol Cancer 2013;12:38.
49. Favre-Bonvin A, Reynaud C, Kretz-Remy C, Jalinot P. Human papillomavirus type 18 e6 protein binds the cellular pdz protein tip-2/gipc, which is involved in transforming growth factor beta signaling and triggers its degradation by the proteasome. J Virol 2005;79:4229–37.
50. Lee DK, Kim BC, Kim IY, Cho EA, Satterwhite DJ, Kim SJ. The human papilloma virus e7 oncoprotein inhibits transforming growth factor-beta signaling by blocking binding of the smad complex to its target sequence. J Biol Chem 2002;277:38557–64.